GE Oil & Gas

Cosimo Bianchini, Ergon Research s.r.l.
Riccardo Da Soghe, Ergon Research s.r.l.
Lorenzo Cosi, GE Oil & Gas
Enzo Imparato, GE Oil & Gas

DOWNSTREAM TECHNOLOGY SOLUTIONS | PRODUCTS & SERVICES

Numerical Analysis of Unsteady Loads on a Steam Turbine Double Seat Control Valve

Abstract

The quest for the ever-greater operational flexibility of large-scale steam turbines continues to drive enhanced control valve design. Such components, subjected to large static loads, also may experience strong vibrations due to unsteady turbulent fluctuations downstream of the throttling section. Challenging design efforts are required to ensure that these fluctuations are confined far from structural natural frequencies through the entire range of operating conditions.

The following study by GE focuses on a computational analysis of the unsteady steam flow developing within a realistic double-seat control valve used in an industrial steam turbine. Actual operating conditions were considered both in terms of steam inflow pressure and temperature, and in terms of flow rates and plug height. Three plug heights were considered: two corresponding to an almost closed plug (thus subjected to choked flow), and the third verified at four different steam rates.

To capture the unsteady nature of the flow and verify the fluid-dynamic forcing frequency, the Scale Adaptive Simulation principle was implemented using Ansys® CFX 14.5 code.

Calculations were run using a computational time step of 1e–4 s and an effective simulation window of 0.2 s for time-averaged values and pressure time signals. The unsteady response was monitored by analyzing the frequency spectra of both integral variables (forces and moment on plug), as well as punctual pressure oscillations.

Analysis of the results showed that it is possible to correlate the principal frequency and amplitude with the operating conditions. The Strouhal number based on plug diameter and bulk flow velocity remains constant independent of operating conditions.

Nomenclature

D	Valve diameter
dt	Computational time step
dp	Mean static pressure loss (inlet-outlet)
f	Characteristic frequency
H	Valve lift
k	Turbulent kinetic energy
l	Characteristic length
L	Discharge duct length
L_{RANS}	Characteristic turbulent length for RANS models
L_{Δ}	Characteristic turbulent length based on grid scale
□	Mass flow rate
$□_c$	Critical mass flow rate
Ma	Mach number
p	Static pressure
R_{ij}	Velocity correlations $\overline{u'_i u'_j}$
Re	Reynolds number
St	Strouhal number
U	Velocity
u',v',w'	x,y,z, directed velocity fluctuations

Greeks

ω	Turbulent specific dissipation rate

Acronyms

CFD	Computational Fluid Dynamics
DFT	Discrete Fourier Transform
LES	Large-Eddy Simulation
RANS	Reynolds Averaged Navier-Stokes
SAS	Scale Adaptive Simulation
SST	Shear Stress Transport

Introduction

An increasing demand for operational flexibility is driving the need for design improvements in large- and medium-scale steam turbines. The key factor affecting design decisions is frequent partialization caused in part by fluctuating availability of renewable power sources, which are ceaselessly enlarging their contribution to global power generation. Additionally, partialization occurs when steam turbines are used for decentralized purposes or mechanical drive applications that require rapid adjustment to consumption power loads. These requirements affect the design of many components that will face off-design conditions for a large part of their lifetime, but above all become critical for the main control valve. This valve regulates the overall pressure ratio available for steam expansion, thus determining the operating conditions of the entire machine.

To control the steam flow entering the turbine, throttle valves typically are positioned axially to achieve the desired governor control function. The shutters usually are linked with a common lift bar (see Figure 1), which when moved radially regulates steam output. The relative position between each shutter and the lift bar is fixed, and is selected based on the number of valves and the steam flow range for different working conditions.

The use of a common lift bar design with governing nozzle groups can cause problems due to oscillating flows in the steam control diffuser valve at critical operation conditions. Ultimately, this can lead to the failure of the plug or stem and damage the steam control valve [2]. This situation is common during turbine startup when large pressure differentials are experienced across the valves and there are very small openings at the valve seat. In this scenario, large pressure drops occur across the valves and high local steam Mach numbers result. To allow for a wider range of performance that maintains safety and reliability, a more complex mechanism for controlling mass flow through the steam turbine is needed.

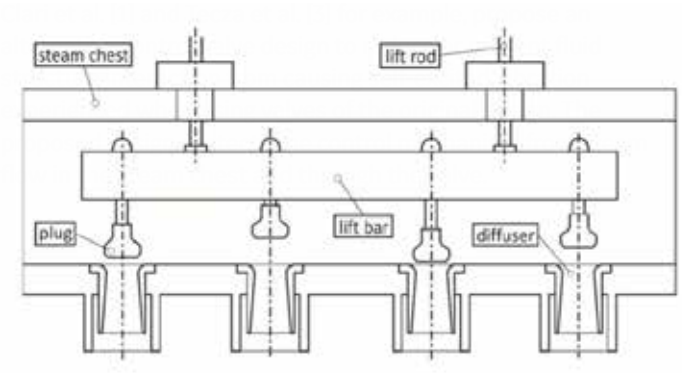

FIGURE 1 Lift bar design with four valves [1]

Liu et al. [4] studied the pressure drops across these valves through experimental investigation and numerical simulation. Based on the analysis of control valve thermodynamic processes, they inferred a relationship between the flow coefficient, area ratio of the valve outlet section to the seat diameter section, and the pressure ratio and total pressure loss coefficient. The relative deviations between formula results and experimental results were found to be within 3 percent. The report also stated that systematic measurement results indicate that the control valve operates steadily when the Mach numbers at the valve inlet and outlet sections are less than 0.15. On the other hand, stem vibration is registered for pressure ratios between 0.8 and 0.4.

In addition, Morita et al. [5] investigated the problem of stem vibration, including both computational and experimental analysis. The team performed Large Eddy Simulation of the air flow within a pipe duct throttled with an emi-sphere plug head, revealing that this numerical setup compares well with unsteady pressure measurements on the valve and the valve seats. A later expanded analysis included real steam flows and found that both gases resulted in the same rotating pressure fluctuations, and the amplitude of such fluctuations increases with the lift while the propagation frequency decreases [6].

More recently Zanazzi et al. [7] performed a numerical investigation of the unsteady behavior of a steam turbine partition valve in throttling conditions. This work compared a simplified in-house procedure with full 3-D Computational Fluid Dynamics (CFD) analysis and experiments available for a single seat valve with axisymmetric stem under a large number of working conditions characterized by five different unsteady modes. The team was able to accurately reproduce the forcing frequencies despite the fact that the CFD procedure strongly underestimated pressure amplitudes.

The study covered here moves beyond the above cited works to investigate the unsteady forces acting on the stem and the chest of a double seat valve used to regulate medium-sized (up to 80 MW) steam turbines for mechanical drive applications (such as those used in an oil refinery). In particular, the study analyzed whether the main fluid dynamic modes excite the natural frequencies of the structure to prevent possible resonance phenomena. 3-D computations were used to resolve the mean and fluctuating turbulent flow field. Due to limitations in the available computational resources, direct resolution of the turbulent field for the configuration of interest was not feasible. A hybrid method, based on the Scale Adaptive Simulation (SAS) technique, was thus implemented to determine the unsteady aerodynamic loads of large-scale turbulent structures. Several operating conditions were analyzed ranging from an almost closed shutter with choked flow to a fully open valve at maximum flow rate. The unsteady behavior of the flow is described by monitoring pressure signals at various locations and analyzing their spectral distribution.

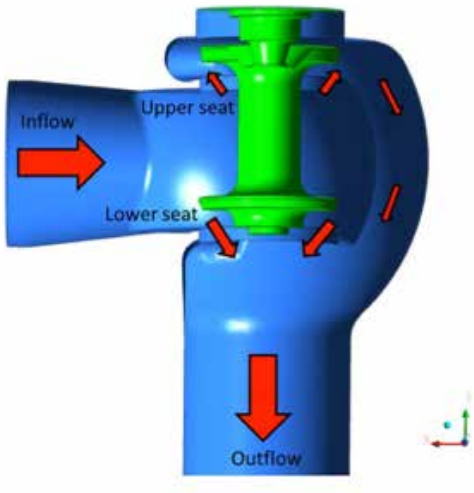

FIGURE 2 Overview of double seat valve geometry

Investigated Cases

This study focused on the double seat valve (shown in Figure 2) composed of a radial admission duct that feeds the axial turbine through two annular orifices regulated by the same two-plug stem. The lower seat directly admits the steam to the main discharge duct, while the upper one is collected by a spiral that surrounds the internal steam chest.

The valve was investigated with the stem opened at three different heights above the seat (H/D = 0.040, 0.153, 0.404), representing two startup configurations and full load positioning. In terms of flow conditions, the two closed plug cases were investigated with a large pressure drop generating fully choked throats as encountered in standard startup procedure.

	Inlet Mach	Inlet Reynolds	H/D
	10^{-2}	10^{6}	
Case 1	1.948	10.96	0.040
Case 2	7.353	41.24	0.153
Case 3	9.105	53.64	0.404
Case 4	13.206	64.55	0.404
Case 5	9.376	24.27	0.404
Case 6	14.064	85.67	0.404

Table 1 Investigated Cases

The wide-open valve configuration was employed under a variety of conditions among which four different simulations were performed to represent the entire range of interest. A summary of investigated flow conditions was reported in Table 1 as a function of inlet Mach and Reynolds number, as well as stem positioning.

Numerical Methods

Turbulence Modeling

As the unsteady features of the turbulent field were of principal importance to this analysis, the use of Large Eddy Simulation (LES) seemed the natural modeling technique. In addition to its more theoretical adherence to turbulent flow physics, LES has proven to better represent the fluctuating behavior of fundamental flows (such as the flow around bluff bodies [8, 9]) than corresponding unsteady RANS computations. However, the use of LES for industrial turbine device simulations is limited to specific applications – often those involving simplified geometries and low Reynolds number flow, due to the high computational requirements. As a matter of fact, LES has been mainly applied to gas turbines rather than to steam turbines [10, 11]. As the prohibitively high computational cost of LES for industrial devices is mainly related to the near wall region, hybrid RANS-LES models have been developed in the course of the last few years to combine the strengths of the two approaches solving the attached boundary layer with RANS and leaving the identification of anisotropic flow structures (such as separated flows) to LES.

Among these hybrid methods, some of the most effective for unsteady aerodynamic flows are those derived from the Scale Adaptive Simulation principle, which sensitizes eddy viscosity RANS models to resolved turbulent scales. The main idea, first proposed by Rotta [12] and later adopted by Menter and Egorov [13], locally compares the smallest resolved fluctuating scales (L_{Δ}) proportional to grid dimension to the RANS characteristic turbulent length (L_{RANS}) and adjusts the turbulent model to recover pure LES treatment when $L_{\Delta} < L_{RANS}$. This idea can be applied theoretically to any turbulence model, although most applications of the SAS principle are conducted on the basis of the k – ω SST model following the work of Menter and Egorov [14]. This work, based on the procedure proposed and validated by Zanazzi et al. [7], exploits the k – ω SST SAS model in the version implemented within the commercial CFD code Anysys CFX v14.5. Further details on model mathematics can be found in [15].

Numerical settings

To perform the proposed investigation, the unsteady turbulent flow solver available in Ansys CFX v14.5 was used. The solver is based on a coupled approach that solves for the pressure-velocity coupling using a time marching technique that, for unsteady computations, implements an inner iterative loop to solve non-linearities. A physical time step (dt = 1e–4s) was chosen based on physics and computational efficiency considerations. The convergence tolerance obtained on the single timestep was around 1e–4 for momentum and 1e–5 for continuity, obtained with a maximum number of three iterations per time step. To obtain converged statistics and increase the investigated spectra, the total simulation time was extended by more than 0.4 seconds for a total of more than 4,000 time steps. Transient effects due to initialization were purged, and time averaging and signal monitoring were activated after 0.2 seconds. For direct resolution of turbulent flows, the highest available order of discretization for both convective and time advancement terms was used to take advantage of the high resolution formulation and to improve solver robustness. In terms of modeling, except for the already mentioned SAS turbulence model, the steam in this analysis was modeled as a homogeneous rarefied gas following ideal gas law. Despite being substantially isothermal, the total energy equation was solved with adiabatic conditions on all the walls to consider the thermal gradients generating due to acceleration within the valve throat, which in choked cases is quite relevant.

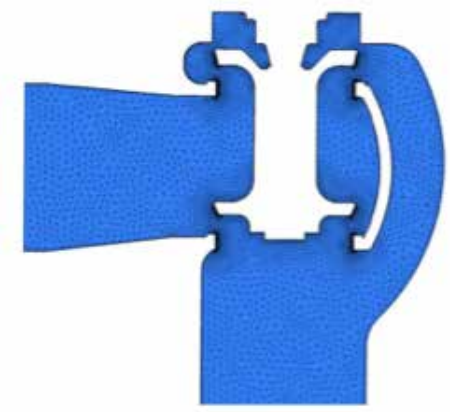

FIGURE 3 Overview of computational grid
(a) Details of computational grid on symmetry plane

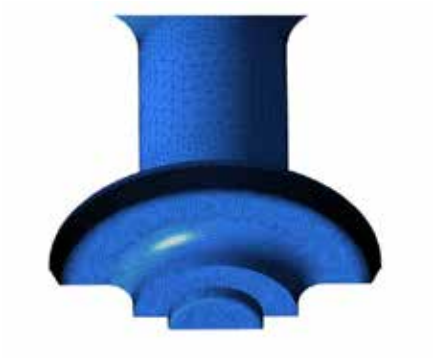

FIGURE 3 Overview of computational grid
(b) Details of computational grid on valve stem

Computational setup

The computational domain employed in this analysis extends in the upstream direction up to the steam chest inflow section, while downstream the discharge duct is extruded for L > 10D to avoid backflow or any interaction with the boundary condition.

In principle, the use of symmetry conditions should be avoided for turbulent flows. This is because turbulent flows are symmetric only in a time-averaged sense, while the instantaneous flux across the plane of symmetry is not zero.

However, for the purposes of this study, computational costs were reduced by forcing the symmetric behavior through boundary conditions. To verify the applicability of this assumption, the full 360° geometry was simulated for Case 1, showing that the flow field within the valve exhibits an almost symmetrical behavior, not only in terms of the time-averaged flow field but also in terms of turbulent fluctuations. In fact, the time averaged velocity correlations (as shown in Figure 5) involving Z-directed fluctuations assume values one order of magnitude lower than the corresponding in-plane oscillations on the symmetry plane.

Furthermore, forcing symmetric behavior by means of boundary conditions does not significantly alter principal mode frequencies that may be identified easily at the monitor points showing a coherent signal. For example, Figure 4 shows the pressure signals registered both for the 180° and the 360° model on a probe positioned close to the stem near the upper seat and located on the symmetry plane.

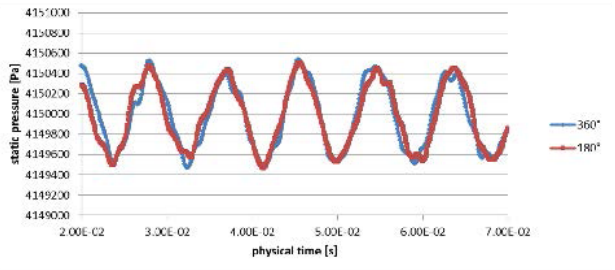

FIGURE 4 Pressure signals for monitor point Up_Stem_In 0 Case 1 - 360° vs 180° model

A very good agreement between the two curves was found, demonstrating that the effects of the symmetry plane are limited to an additional filter on high frequency noise that results slightly damped in the 180° model. The focus of the analysis was on large fluctuating structures that are more dangerous for resonance of the solid structure and fatigue considerations rather than aerodynamically generated noise. Therefore, subsequent simulations were conducted exploiting the symmetry constraint to reduce computational costs to an affordable level.

The three employed meshes were generated using the same procedures and criteria: hybrid element shape such as tetrahedral in the free stream with five layers of prisms along the walls to discretize boundary layer and fine grid clustering in the throat and on the stem. Near-wall grid size was chosen to maintain first node dimensionless wall distance (y+) below 300 to fulfil wall function requirements on most of the walls, and in particular in the proximity of the throttling section. To permit the direct resolution of an adequate amount of turbulent fluctuation, the meshes are composed of 14 million cells distributed in the domain (see Figure 3) with limited coarsening in the freestream region. Employed grids offer high quality elements as the averaged orthogonality angle is above 70° and the mesh expansion factor is less than three.

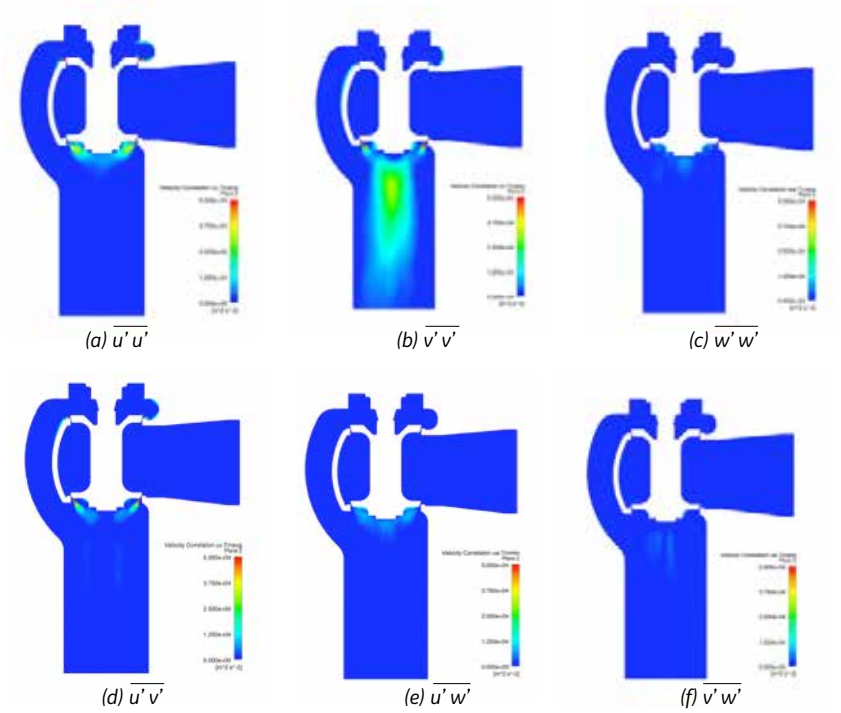

FIGURE 5 Time-averaged velocity correlations on symmetry plane

Data analysis

Turning 3-D computations of turbulent flows into values that help characterize the unsteady behavior of the fluid is not particularly straightforward. This is due to both the large amount of data produced and the chaotic nature of turbulence that makes the analysis of principal flow structures a challenging task. In this study, for example, the work was dedicated to an estimate of the fluctuating aerodynamic forcing acting on the stem and the steam chest to verify possible interaction with the structure eigenmodes. It was simply not practical to collect instantaneous pressure fields on all computational nodes of the surfaces of interest for the entire simulated time. Apart from problems arising due to the size of the dataset, time signals contain contributions pulsating at different frequencies, which are difficult, or virtually impossible, to analyze in the time domain.

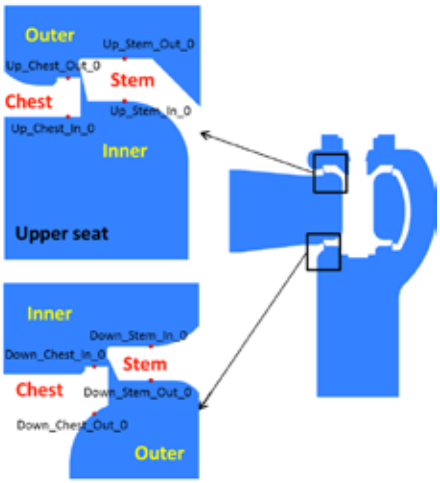

FIGURE 6 Pressure probe positioning

To fully and simply characterize the main forces acting on the valve, the pressure signal was registered in a reduced set of nodes together with global forces and moments acting on the stem. Most interesting locations were identified on overhung structures, such as the stem plug and the chest narrowing. As depicted in Figure 6, eight different positions were selected to be representative of pressure loads on the shutter and on the external structure. For each position, nine probes were distributed tangentially with a spacing of 22.5° for a total of 72 pressure signals registered. To more easily identify the monitor points, they were named with a composite word identifying the nearest seat (Up/Down), closest surface (Stem/Chest), relative position with respect to the valve throat (In/Out) and, finally, the angular coordinate (such as Up Stem Out 45). Discrete Fourier Transform then was applied to every local signal to highlight the principal frequencies, relative phase of fluctuations, and interactions between different zones of the domain.

With the above-mentioned numerical setup, frequencies ranging between 5 and 5,000 Hz were analyzed, providing a sufficient resolution to properly characterize the range of interest (10-1,000 Hz).

TIME AVERAGED AERODYNAMICS

The first thing to verify was how the different operating conditions affected the time-averaged flow within the valve. Figure 7 shows an example of mean velocity contour plots on the symmetry plane. The simulated time window was sufficient to obtain converged statistics as the contours do not show any corrugation caused by turbulent eddies.

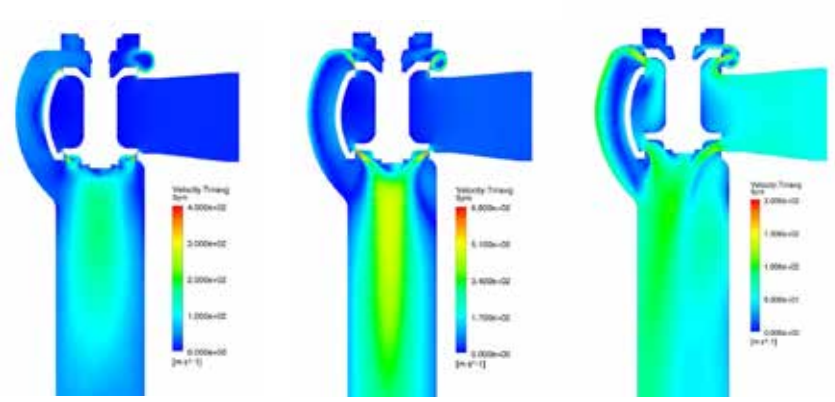

(a) Case 1 *(b) Case 2* *(c) Case 3*

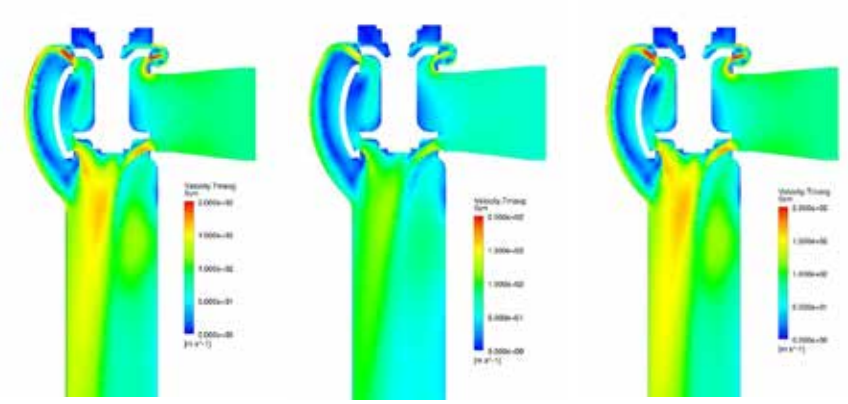

(d) Case 4 *(e) Case 5* *(f) Case 6*

FIGURE 7 Time-averaged velocity field on symmetry plane

The two choked conditions were characterized by an almost symmetric flow distribution within the discharge duct. With such a small gap between stem and chest, the pressure drop across the throat was large enough to guarantee tangentially uniform conditions to the annular jet. Furthermore, the throat passage area of the upper seat was substantially less than the lower one, causing a strong reduction of steam mass flow in the spiral. Only about 33 percent of the total injected steam flowed through the upper seat.

Gas coming from the spiral is characterized by low momentum due to the lower mass flow blown through the upper seat and the diffusion effect within the spiral itself. The main annular jet issued by the lower seat is therefore not deeply influenced by the steam collected within the spiral. Despite showing identical flow features in the lower seat, the behavior of the upper valve was quite different among the two closed conditions. Steam jets at H/D = 0.04 were strongly bent in the radial direction and evolved attached to the inner casing. However, steam jets at H/D = 0.153 impinged on the external casing, and flowed toward the discharge duct along this wall.

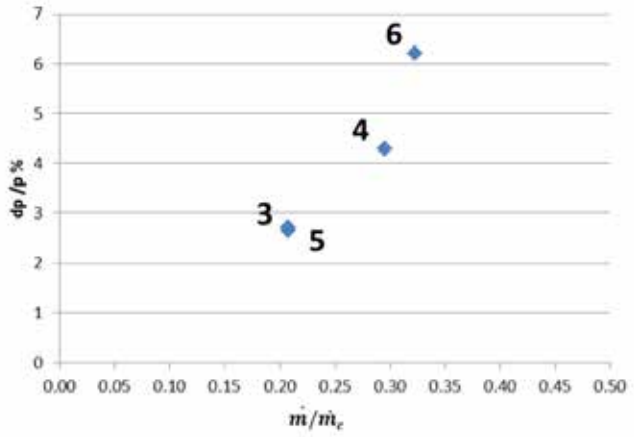

FIGURE 8 Double seat valve characteristic response

When the valve was open, the effect of lateral feeding was evident, and the lower seat annular jet bent toward the concordant side of the duct due to non-uniform admission in the stem throat. In addition, the flow split between the upper and lower valve was balanced almost perfectly. A second velocity peak, although less intense, was registered on the discordant side. This peak also was caused by steam collected by the spiral.

To help estimate the pressure losses necessary to guarantee a certain mass flow, it was useful to report the characteristic curve of the valve at wide open position. Figure 8 depicts the obtained mean pressure drop as a function of reduced mass flow. It shows values between 2.2 and 6.2 percent for 0.2 < □/□$_c$ < 0.4 (quite high losses for an open admission valve [16, 17]). Indeed, critical mass flow was calculated using a rough estimate of the throat area based only on geometrical reasoning. While this technique may be quite simplistic for a complex turbulent 3-D flow, it is believed to be a representative value due to the thin boundary layers developing at such a high Reynolds number. In addition, possible errors in this type of evaluation affect all conditions in nearly the same manner.

UNSTEADY LOADS

Because the global behavior of the unsteady steam flow within the valve had to be extracted from a huge amount of data, the discussion of obtained results focused on Discrete Fourier Transform analysis of the registered pressure signals. Figures 9 and 10, for example, show frequency spectra of the probes located at two representative locations (Up_Chest_Out and Down_Stem_In). Different curves correspond to different tangential positions.

The internal fluctuations (such as those shown in Figure 10) were characterized by a lower broadband contribution, and main peaks were clearly identifiable. The external fluctuations (such as those shown in Figure 9) presented higher peak amplitudes and a larger spread on frequency band. However, significant contributions were limited for all probes and for each investigated case in the range of 10-1000 Hz. An exception to this general trend was noted in Case 2, reported in Figures 9(b) and 10(b), but only due to the very large pressure fluctuations that arise outside the inner chamber and reach values as high as 80 kPa. Furthermore, the pressure signals at the various probes along the same circumference were consistent with each other, with perfectly matched peak frequencies and only slight deviations in amplitude.

	Inner probes	Outer probes
	Hz	**Hz**
Case 1	116	106
Case 2	113	280
Case 3	25	25
Case 4	30	30
Case 5	30	30
Case 6	35	35

Table 2 Principal Frequencies

It is interesting to extract from the obtained spectra (including those not shown in this report), a characteristic frequency that is intended as the first frequency characterized by a significant peak, both for inner and outer probes. These principal frequencies were reported in Table 2, and show how, at least for subsonic cases, throat acceleration was not sufficient to acoustically decouple the upstream and downstream region. For Cases 3 to 6, internal and external frequencies were equal and presented very small variations around the same value. However, in Cases 1 and 2, the outer probes were fluctuating more independently, in one case displaying slightly lower characteristic frequency and in the other a value higher than second harmonic.

The obtained frequencies for the inner probes can be roughly grouped in two homogeneous subsets characterized by values around 115 Hz for the choked cases and 30 Hz for the subsonic cases. This grouping made it convenient to use the performed run to propose a simple model based on geometry and flow conditions that could provide a first estimate of the characteristic frequency of the fluid forcing, which could help at early design stage. To better understand the relevant parameters, a set of characteristic velocities and lengths were combined to calculate various dimensionless expressions defined as Strouhal numbers (St = l · f /U). For the velocity, both the

sound speed (acoustic) and the bulk steam velocity in the throat (aero) were used. In terms of length scales, the upper and lower gaps as well as the stem diameter were employed. This allowed for six different Strouhal to be computed (as plotted in Figure 11 in a log-log graph for the inner probes). The only Strouhal that showed results of the same order of magnitude for every tested condition was that defined on the aerodynamic velocity in the throat and the stem diameter. With a constant value of St=0.15 obtained by averaging the six investigated cases, it was possible to evaluate characteristic internal frequencies with an average error of 10 percent, which is generally compatible with safety coefficients employed by structural designers to avoid dangerous interactions with structure eigenfrequencies.

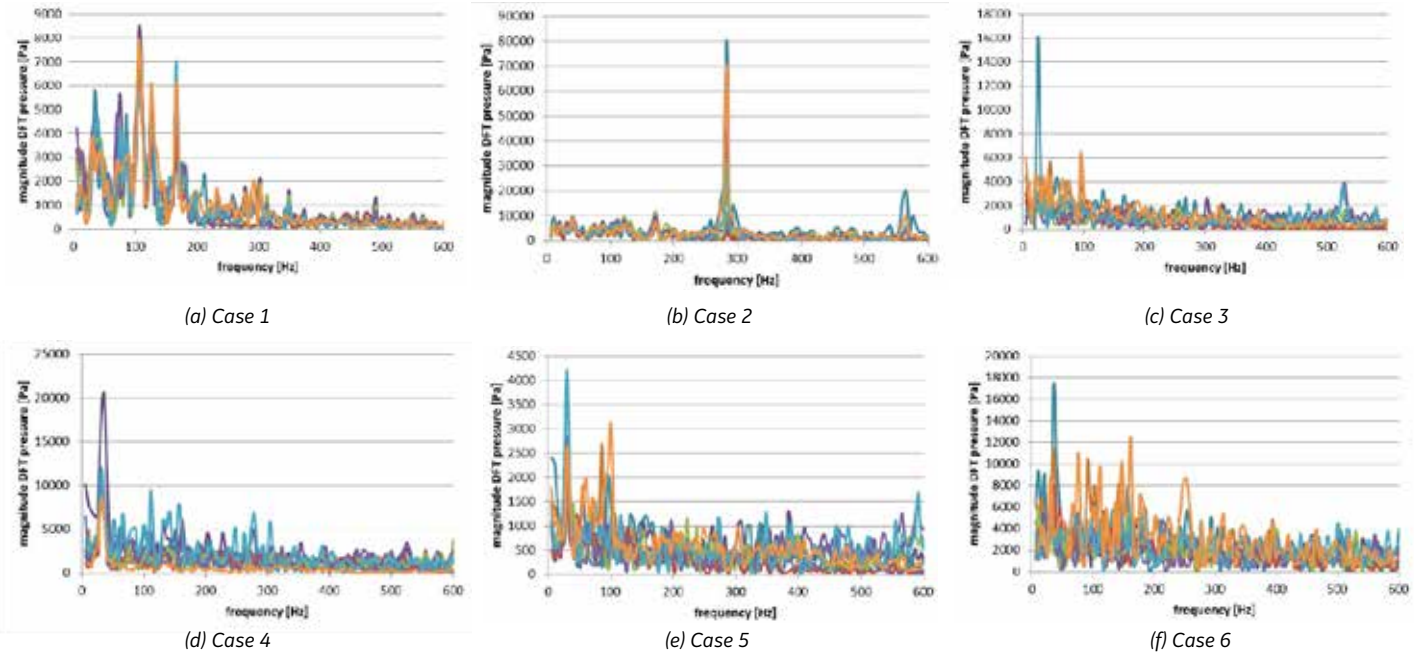

(a) Case 1 *(b) Case 2* *(c) Case 3*

(d) Case 4 *(e) Case 5* *(f) Case 6*

FIGURE 9 Amplitude DFT pressure signal on Up Chest Out probes

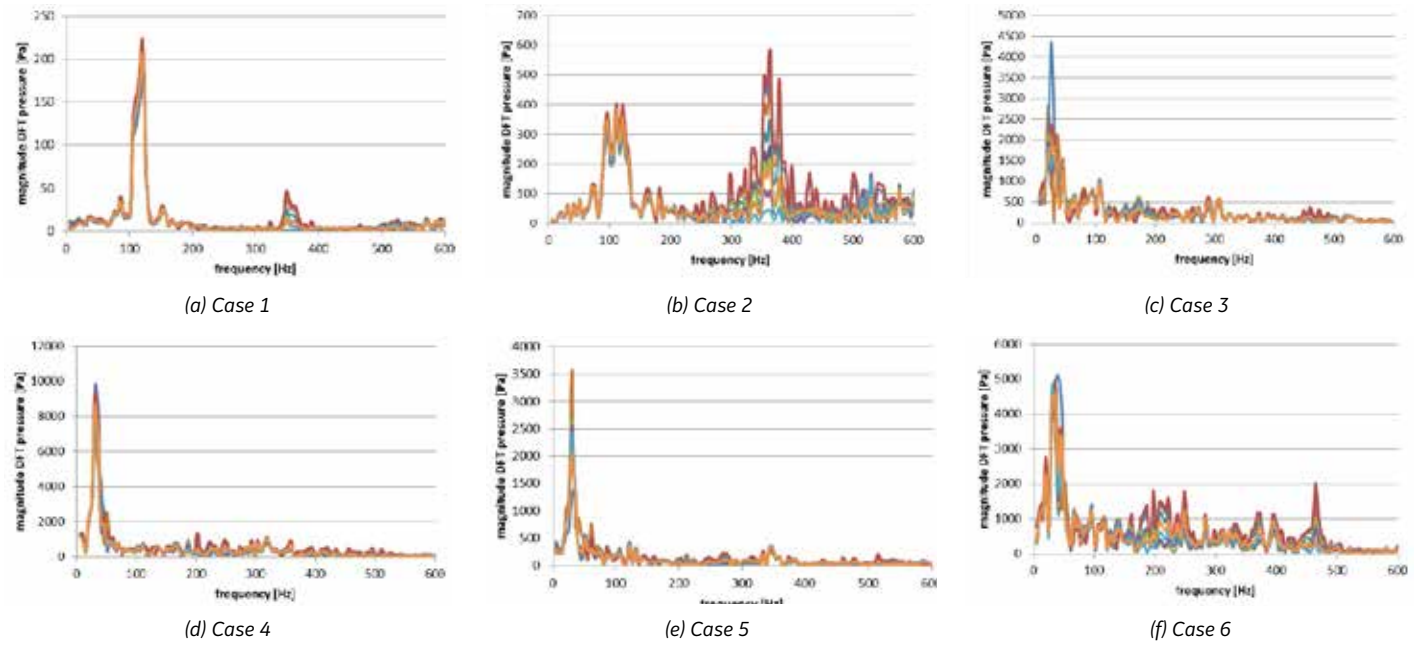

(a) Case 1 *(b) Case 2* *(c) Case 3*

(d) Case 4 *(e) Case 5* *(f) Case 6*

FIGURE 10 Amplitude DFT pressure signal on Down Stem In probes

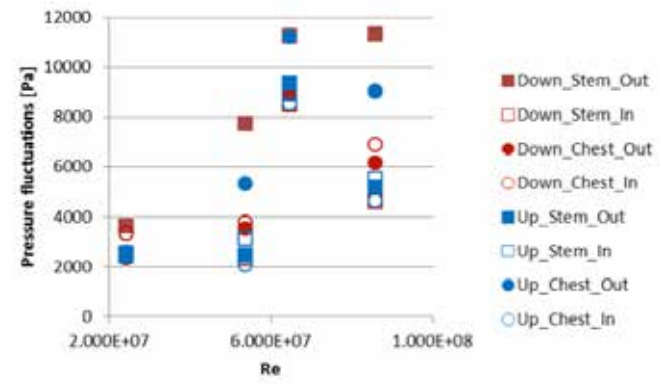

FIGURE 11 Strouhal number evaluation for inner probes

Also, in terms of peak amplitudes, the two groups of subsonic and choked cases behaved differently. For the supersonic cases, the inner chamber was almost steady while the amplitude of fluctuations due to the annular jet was large, reaching values higher than 40 kPa as a tangential average, resulting in fluctuations nearly four times greater than for the most critical subsonic case. On the other hand, as expected, the subsonic cases showed a stronger link between internal and external oscillation magnitude. Outer fluctuations were limited to nearly double the amount of their respective upstream homologous probes. To provide a description of how these pressure fluctuations depend on operating conditions and probe position, a maximum Fourier coefficient was averaged tangentially for each position and plotted (see Figure 12) against the Reynolds number for the subsonic cases. The lower seat was subjected to higher unsteady loads than the upper one – in particular those directed on the stem of the valve – which shows an increasing trend with Reynolds number. This fluctuation is propagated toward the other probe positions with attenuation proportional to fluid reference density, which regulates flow inertia. As a consequence, Cases 3 and 6, which correspond to Re = 5.36 · 1e7 and 8.57 · 1e7 respectively, resulted in lower minimal oscillation. Note that the upper seat, due to its shaping, excites the chest much more than the stem.

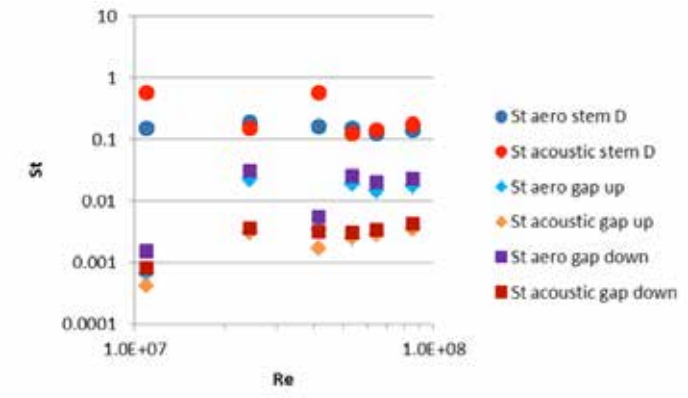

FIGURE 12 Fluctuation amplitudes for subsonic cases

CONCLUSIONS

An unsteady CFD analysis was performed to analyze the oscillating aerodynamic loads acting on the stem and the chest of a double seat partition valve operating upstream of the impulse stage of a medium-size industrial steam turbine. Actual geometries and representative flow conditions, ranging from choked throat to open valve configurations, were considered. The analysis was carried out using hybrid turbulence modeling based on the Scale Adaptive Simulation principle. Unsteady forces were computed by performing spectral decomposition of monitored pressure signals at selected points.

Obtained results allowed different behaviors to be identified for the subsonic and the choked conditions, both in terms of main frequencies and amplitude of oscillations. Coherent fluctuations were observed inside and outside the steam chest in the subsonic cases. When the throat was sonic, inner pressure oscillations were very low while outer oscillations were amplified due to the higher annular jet momentum. In terms of principal frequencies, the Strouhal number based on bulk flow velocity and stem diameter was invariant among the investigated cases. Thus, the Strouhal number can be used to extend obtained findings to other operating conditions, predicting a priori proper frequency of the aerodynamic forcing.

References

1 Clari, M. B., Polklas, T., and Joos, F., 2011. "Three- dimensional flow separations in the diffuser of a steam turbine control valve". ASME Conference Proceedings, 2011(54679), pp. 2327–2334.

2 Hardin, J., Kushner, F., and Koester, S., 2003. "Elimina- tion of flow-induced instability from steam turbine control valves". Proc. of the 32nd Turbomachinery Symposium, pp. 99–108.

3 Tecza, J., Chochua, G., and Moll, R., 2010. "Analysis of fluid-structure interaction in a steam turbine throttle valve". ASME Conference Proceedings, 2010(44021), pp. 2329–2338.

4 Liu, G., Wang, S., Guo, H., Mao, J., Feng, Z., and Xiang, X., 2008. "Investigation on flow characteristics and stability of control valves for steam turbines". ASME Conference Proceedings, 2008(43154), pp. 811–820.

5 Morita, R., Inada, F., Mori, M., Tezuka, K., and Tsujimoto, Y., 2004. "CFD calculation and experiments of unsteady flow on control valve". ASME Heat Transfer Fluids Engineering Summer Conference, 2004(HT-FED04-56017).

6 Morita, R., and Inada, F., 2007. "Pressure fluctua- tions around steam control valve: Steam experiments and CFD calculations". ASME Conference Proceedings, 2007(26444), pp. 421–427.

7 Zanazzi, G., Schaefer, O., Ridoutt, C., and Sell, M., 2013. "Unsteady CFD simulation of control valve in throttling conditions and comparison with experiments". ASME Con- ference Proceedings, 2013(94788).

8 Rodi, W., 1997. "Comparison of LES and RANS calculations of the flow around bluff bodies". Journal of Wind Engineering and Industrial Aerodynamics, 69(71), pp. 55–75.

9 Sohankar, A., Davidson, L., and Norberg, C., 2000. "Large Eddy Simulation of flow past a square cylinder: Comparison of different subgrid scale models". Journal of Fluids Engineering, 122, pp. 39–47.

10 Wang, S., Yang, V., Hsiao, G., Hsieh, S., and Mongia, H. C., 2007. "Large-Eddy Simulations of gas-turbine swirl injector flow dynamics". J. Fluid Mech., 583, pp. 99–122.

11 Staffelbach, G., Gicquel, L., and Poinsot, T., 2006. "Highly parallel Large Eddy Simulations of multiburner configurations in industrial gas turbines". Lecture Notes in Computational Science and Engineering, 56.

12 Rotta, J. C., 1972. Turbulente Strömumgen. BG Teubner Stuttgart.

13 Menter, F. R., Egorov, Y., and Rusch, D., 2006. "Steady and Unsteady Flow Modelling Using k-√kL Model". Proc. Turbulence, Heat and Mass Transfer 5, K. Hanjalic, Y. Nagano and S. Jakirlic (Editors).

14 Menter, F. R., and Egorov, Y., 2005. "A Scale-Adaptive Simulation model using two-equation models". AIAA paper 2005-1095.

15 Menter, F. R., and Egorov, Y., 2007. "Development and Application of SST-SAS Turbulence Model in the DESIDER Project". Advances in Hybrid RANS-LES Modelling, Shia- Hui Peng and Werner Haase (Editors), Springer 2008.

16 Bianchini, C., Micio, M., Tarchi, L., Cortese, C., Imparato, E., and Tampucci, D., 2013. "Numerical analysis of pressure losses in diffuser and tube steam partition valves". ASME Conference Proceedings, 2013(95527).

17 Du, X., and Gao, S., 2013. "Numerical study of complex turbulent flow through valves in a steam turbine system". International Journal of Materials, Mechanics and Manufacturing, 1(3).

Imagination at work

GE Oil & Gas - Global Headquarters
The Ark - 201 Talgarth Road, Hammersmith - London, W6 8BJ, UK
T +44 207 302 6000
customer.service.center@ge.com

Nuovo Pignone S.p.A. - Nuovo Pignone S.r.l
Via Felice Matteucci, 2 - 50127 Florence, Italy
T +39 055 423 211
F +39 055 423 2800

Downstream Technology Solutions
4424 West Sam Houston Parkway North - Houston, TX 77041-8200, US

Numerical Analysis of Unsteady Loads on a Steam Turbine Double Seat Control Valve
Cosimo Bianchini, Riccardo Da Soghe, Lorenzo Cosi, Enzo Imparato

GEA31929 (07/2015)